

# Estimating Total Solar Irradiance during the 21st century

Victor Manuel Velasco Herrera,<sup>1</sup> Blanca Mendoza<sup>1</sup> and Graciela Velasco Herrera.<sup>2\*</sup>

<sup>1</sup>*Departamento de Ciencias Espaciales, Instituto de Geofísica, Universidad Nacional Autónoma de México, Ciudad Universitaria, Coyoacán, 04510, México D.F., MÉXICO and*

<sup>2</sup>*Centro de Ciencias Aplicadas y Desarrollo Tecnológico, Universidad Nacional Autónoma de México*

The reconstruction and prediction of solar activity is one of the current problems in dynamo theory and global climate modeling. We estimate the Total Solar Irradiance for the next hundred years based on the Least Square Support Vector Machine. We found that the next secular solar minimum will occur between the years 2003 and 2063 with an average of  $1365.4 \text{ W/m}^2$  close to the Dalton or Modern minima. We calculate the radiative forcing between the modern maximum and the 21<sup>st</sup> century minimum to be  $-0.1 \text{ W/m}^2$ .

The modern comprehension of solar variability possibly began when Schwabe published the periodicity of sunspots in 1843 [1]. In 1894, Maunder published a discovery that has maintained the Solar Physics in an impasse. In his famous work on “A Prolonged Sunspot Minimum” Maunder wrote [2]:

“The sequence of maximum and minimum has, in fact, been unfailling during the present century [...] and yet there [...], the ordinary solar cycle was once interrupted, and one long period of almost unbroken quiescence prevailed”

The Maunder’s discovery went unnoticed and forgotten until 1976 when Eddy brought it to light again [3]. The existence of prolonged solar minima has been one of the most controversial questions in Solar Physics. However the possibility of prediction of new periods of diminished solar activity is even more controversial.

To estimate future solar activity, several methods have been used, for instance dynamo models, spectral methods, regression methods or neuronal network methods [4]. These estimations have in common that they are applied to short-time reconstructed series and that they do not discuss the relative accuracy of the methods.

The fluctuations of the solar time series is a tool that helps to study the solar magnetic field as well as to understand the solar dynamo. These fluctuations can occur for instance in the amplitude, phase, frequency, energy and power of the solar phenomena.

The majority of solar activity analysis focuses on fluctuations of the amplitude. In this paper, we propose to consider not only the fluctuations in amplitude but also in the power of the Total Solar Irradiance (TSI) as a physical measure of the energy released by the solar dynamo, which contributes to understand the nature of ‘profound solar magnetic field in calm’. Regardless of the mechanism that produces solar activity minima (stochastic, chaotic, intermittent or quasi-periodical processes), the study of these minima is very important for the solar dynamo theory, as well as for its impact on solar-terrestrial relationships [5, 6].

Recent studies suggest that the mid-term (1 – 2 years) and the secular periodicities are the product of chaotic quasi-periodic processes and not of stochastic processes or intermittent process [7, 8]. Different spectral analysis of solar activity series [8, 9] show several significant long-term periodicities. It is also known that the solar cycle (Schwabe periodicity [1]) varies cyclically with a mean period of about 11-years and the magnetic cycle (Hale cycle [10]) with a mean period of about of 22-years. This behavior motivates attempts to predict solar activity, especially now that an unexpectedly low activity solar cycle 23 occurred and could be the sign of the beginning of a new secular solar minimum [8]. The behavior of the solar cycle 23 minimum has shown an activity decline not previously seen in the past cycles for which spatial observations exist [11–14].

The descending phase and minimum measurements of solar cycle 23 show that in particular the TSI has fallen below the previous two solar minima values: the mean PMOD composite TSI for September 2008 is  $1365.26 \pm 0.16 \text{ Wm}^{-2}$ , compared to  $1365.45 \text{ Wm}^{-2}$  in 1996 or  $1365.57 \text{ Wm}^{-2}$  in 1986 [15].

Over the 11-years solar cycle, TSI variations of  $\sim 0.07\%$  have been observed between solar minimum and maximum [16]. This modulation is mainly due to the interplay between dark sunspots and bright faculae and network elements [17]. Studies using cosmogenic isotope data and sunspot data [8, 18] indicate that currently we are within a grand activity maximum which began after  $\sim 1930$ .

Studying the solar wind, the interplanetary magnetic field strength and the open solar flux over the past century, Lockwood [19] found that all three parameters show a long-term rise peaking around 1955 and 1986 and then decline, yielding predictions that the grand maximum will end in the years 2013, 2014 or 2027 depending on the parameter used.

Other works indicate that the current maximum will not last longer than two or three solar cycles more [20]. Furthermore, it has been suggested that a Dalton-type minimum has already began in solar cycle 23 reaching [21, 22] to solar cycles 24 and 25, while the Solar Cycle 24 Prediction Panel indicates a lower limit of  $90 \pm 10$  for the

maximum sunspot number [23] of solar cycle 24.

To project the TSI for the next hundred years, we use a method based on Least Squares Support Vector Machines (LS-SVM) with Nonlinear Autoregressive Exogenous (NARX) model and with radial basis function (RBF) kernel that allows a better precision in the estimation of the future values of a time series [24, 25].

Since the instrumental TSI records began in 1979, we work with reconstructed TSI series. Long-term reconstructions of TSI [26, 27] show epochs of maxima and minima when substantial changes in the TSI occur. These changes can contribute to climate variability [28] and new estimate of the TSI for the 21st century, will have an important impact on climate modeling.

We tested three TSI recent reconstructions. Two of them use a model based on the evolution of the Sun's total and open magnetic flux: The Wang reconstruction [29] consider differential rotation, supergranular convection and meridional flow; this model is used to derive two TSI reconstructions, one with and one without a secularly varying background; from 1850 onwards these reconstructions are the recommended solar forcings for the fifth Coupled Model Intercomparison Project 20th century simulations [30].

The Krivova reconstruction [31] relies on time constants representing the decay and conversion of the different photospheric magnetic flux components. The Stenhilber reconstruction [26], uses the observationally derived relationship between TSI and the open solar magnetic field, the latter obtained from the cosmogenic radionuclide  $^{10}\text{Be}$ .

However, the best reconstruction to apply our method is the Krivova reconstruction [31] because it has a better temporal and spectral resolution compared to the Stenhilber reconstruction [26] and the correlation between the reconstructed and the PMOD composite is better than the Wang reconstruction [29].

From 1610 to 1975 we use the Krivova reconstruction

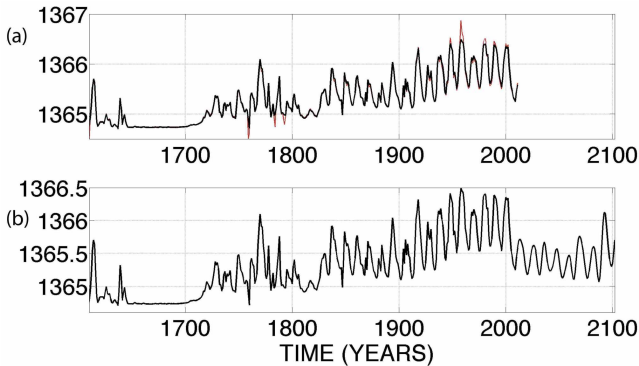


FIG. 1. Time series. (a) The TSI-KRIVOVA-PMOD (red line) from 1610 to 2010 superposed on the times series estimated with the Least Squares Support Vector Machines (LS-SVM) between 1610 and 2010 (black line). (b) The LS-SVM model time series (black line) between 1610 and 2100

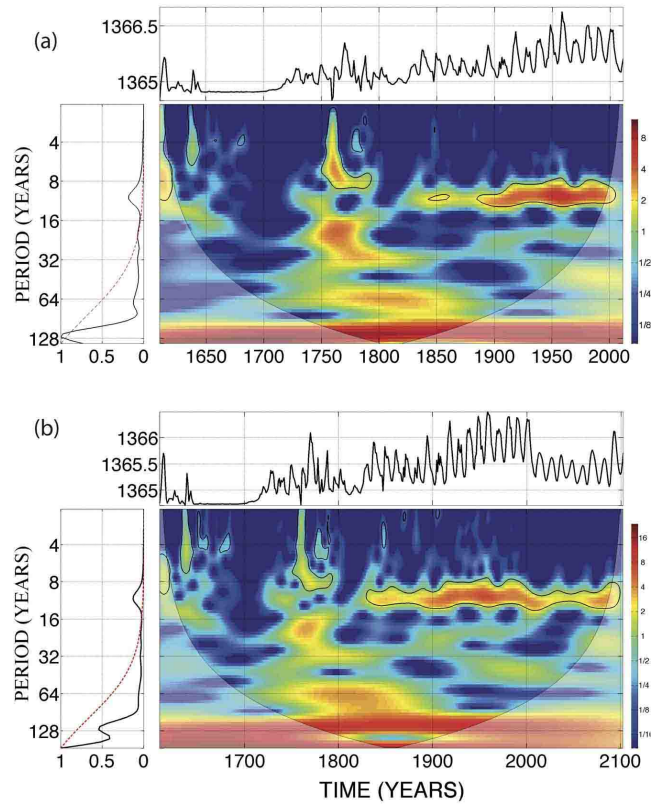


FIG. 2. (a) Upper panel, TSI-KRIVOVA-PMOD; right panel spectral wavelet analysis; left panel global wavelet. (b) The same as in (a) but for the LS-SVM model.

[31] and from 1976 to 2010 we use the PMOD composite. In this work we use the TSI-KRIVOVA-PMOD between 1610 and 2010.

To search for the future TSI values, the NARX LS-SVM was trained with 80% of random data of the TSI-KRIVOVA-PMOD, obtaining a mean squared error (MSE) of 0.0084, the testing of the remaining 20% presents an MSE of 0.0073.

We plot the TSI-KRIVOVA-PMOD with red line and the NARX LS-SVM model with black line in Fig. 1a. It is clear that the NARX LS-SVM model (black line) reproduces very well the TSI-KRIVOVA-PMOD; the linear correlation coefficient between the TSI-KRIVOVA and the NARX LS-SVM model series for 1610-1975 is  $r = 0.9969$ , while  $r$  value for the PMOD and the NARX LS-SVM model for 1976-2010 interval is 0.9959.

In Fig. 1b we present the NARX LS-SVM future TSI estimation (black line) between 2011 and 2100 with standard deviation  $\sigma = 0.4318 \text{ Wm}^{-2}$ . We notice a decreasing trend of the TSI between 2003 and 2063, coinciding with other types of prediction adopting different methods [8, 19, 20, 22].

However, it is not enough to conclude that the amplitudes among the reconstructed, the composite and the modeled time series are similar, it is also necessary to compare the

spectral characteristics.

We apply the wavelet analysis using the Morlet function [32], to quantify the TSI time series till 2100 A.D. and to analyse local variations of multiple periodicities. This method provides a higher resolution of periodicity, allows us to calculate the phase, and to filter the TSI in bandwidths [33].

Also, to calculate the confidence level we used the normalizedpdf function, in this way the TSI will have a gaussian distribution[34]. Wavelet meaningful periodicities (confidence level greater than 95%) must be inside the cone of influence (COI), which is the region of the wavelet spectrum outside which the edge effects become important [35]. We also include the global spectra in the wavelet plots to show the power contribution of each periodicity inside the COI [36].

We established our significance levels in the global wavelet spectra with a simple red noise model (increasing power with decreasing frequency [37]). We only took into account those periodicities above the red noise level.

In Fig. 2 we show the wavelet analysis for the TSI-KRIVOVA-PMOD (Fig. 2a) and the NARX LS-SVM model (Fig. 2b). In the central panel of Fig. 2a the 11-years cycle appears attenuated during the secular minima and is stronger since  $\sim 1875$ , while the  $\sim 120$ -years cycle keeps a more or less uniform power along all the time-span considered, both periodicities appear above the red noise level in the global spectra (right panel). Fig. 2b shows roughly the same spectral evolution of Fig. 2a but the two peaks above the red noise level are the 11-years and the 240-years. Also Fig. 2b indicates that the 11-years cycle will be attenuated during the next 60 years (to 2063), which is a characteristic of a secular minima.

In Fig. 3 we show a further analysis of the amplitudes (black areas) and phases (blue lines), that allow us to quantify the starting and ending of a cycle of the NARX LS-SVM model and were obtained using the inverse wavelet transform [32]. Fig. 3b shows the 11-years cycle, as sunspots were so scarce during the “Prolonged Sunspot Minimum”, it has been suggested that the solar dynamo stopped [5, 6]. The figure clearly shows the 11-years amplitude attenuated during the Maunder, Dalton and Modern minima (negative phase of the periodicity of 120-years in Fig. 3c). The amplitude of the solar cycle never disappears completely, this is particularly so during the Maunder minimum [38]. After the year 2000 the peak amplitude of the cycle tends to decrease, in fact during the 21st minimum (2003–2063) it is similar to the Dalton or Modern minima (1883–1940).

The phase also shows an amplitude modulation, it presents an inversion between  $\sim 1780$  and 1790, as this is not a particularly maximum or minimum time, we suggest that it comes probably from a shortcoming of the TS-KRIVOVA reconstruction in this time-interval.

From 2011 to 2100, the phase does not show any other inversion, probably indicating the good quality of our es-

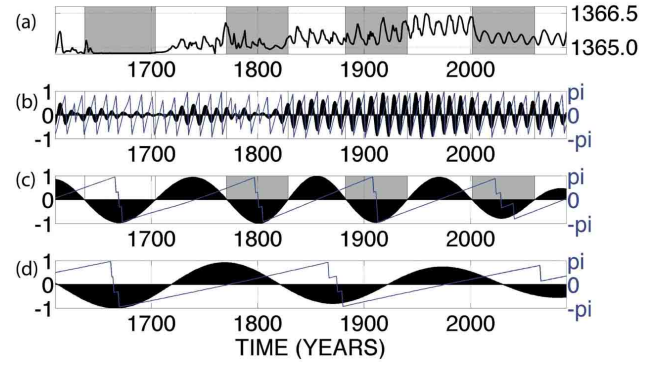


FIG. 3. Phases (blue lines) and amplitudes (black areas) associated to the main periodicities of the LS-SVM model. The light-gray shading indicates the time-span of the secular minima. (a) Modeled time series. (b) The 11-yrs cycle. (c) The 120-yrs cycle. (d) The 240-yrs cycle.

timation. Fig. 3c shows the 120-years cycle, we notice that it is the negative phase of this periodicity that coincides with the secular minima: Maunder between the years 1637–1704, Dalton between the years 1771–1829, Modern between the years 1883–1940 and the 21st century minima between the years 2003 and 2063.

Based on this periodicity we calculate the average TSI for the secular minima: Maunder  $1364.8 Wm^{-2}$ , Dalton  $1365.2 Wm^{-2}$  Modern  $1365.5 Wm^{-2}$  and the 21st century  $1365.4 Wm^{-2} \pm 1\sigma = 0.4318 Wm^{-2}$ , this TSI value is between the Dalton and Modern minima. Again we observe that the phase does not change after 2010.

The Modern maximum noticed between the years 1940 and 2003 has an average TSI of  $1366 Wm^{-2}$ , and the 21st century minimum has a TSI average of  $1365.4 Wm^{-2}$ , this implies a negative radiative forcing of  $\sim -0.1 Wm^{-2}$ . The radiative forcing for the Maunder minimum to the Modern maximum[31] is  $\sim 0.21 Wm^{-2}$ , then the radiative forcing associated to the 21st century minimum is almost half of that forcing.

Finally, Fig. 3d shows the 240-years cycle, it seem that according to the lag between the 120-years and 240-years cycles we have different amplitudes of the secular solar minima, for instance, when its negative phase coincides with the 120-years cycle we have the deepest minima, like the Maunder minimum. Again, the phase of this periodicity holds for the next 100 years.

To decide when the solar activity is “high” or “low”, we calculate the power of the TSI as a direct indicator of energy released by the solar dynamo and the level of activity for each solar cycle. We use the mean power value of the PMOD composite (1976 – 2010) to calculate the anomalies for each cycle. The power anomalies are normalized and appear as blue bars in Fig. 4, which also presents the TSI (solid line). There are positive power anomalies during solar cycles 21 and 22, coinciding with the end of the Modern maximum. Between solar cycles 23 and 30 the power

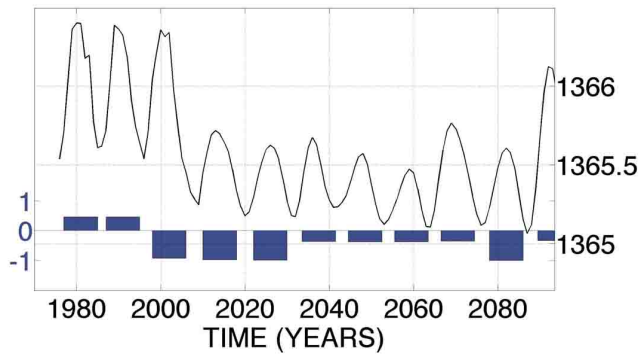


FIG. 4. We use the mean power PMOD composite (1976–2010) to calculate the power anomaly for each cycle. The power anomalies are normalized and appear as blue bars. The TSI is the solid line. Negative (or Positive) power anomalies is “Low” (or “High”) solar activity

anomalies are negative, coinciding with negative phase of the 120-years periodicity. This reinforces the result of Fig. 3c suggesting that this periodicity is closely associated with secular minima. According to the power of the anomalies, solar cycles 23–25 and 30 could present lower activity than cycles 26 to 29, regardless of the fact that the peaks of cycles 27 and 28 are the lowest.

The calculated power anomalies show that low solar secular activity occurs when there are negative anomalies and high solar secular activity appears with positive anomalies. It is possible that the zero in the anomalies, represents the normal state of the dynamo. The “Prolonged Sunspot Minimum” discovered by Maunder, represents a phase of solar history and corresponds to a special state of the dynamo when it is working well below its average power.

This work was partially supported by DGAPA-UNAM, IN103209 – 3, IN117009 – 3, IN105909 and IN117009 grants, IXTLI: IX101010 and IX100810 grants and CONACYT-F282795 grant.

---

\* Electronic address: vmv@geofisica.unam.mx

[1] V. H. H. Schwabe, *Astronomische Nachrichten*, **473**, 283–284 (1843).  
 [2] E.W. Maunder, *Mon. Not. R. Astron. Soc.*, **17**, 173–176 (1894).  
 [3] J.A. Eddy, *Science*, **192** (4245), 1189–1202 (1976).  
 [4] K. Petrovary, *Living Rev. Solar Phys.*, **7** (2010).  
 [5] P. Charbonneau, *Living Rev. Solar Phys.*, **7** (2010).  
 [6] M. Ossendrijver, *Astron. Astrophys. Rev.*, **11**, 287–367 (2003).

[7] B. Mendoza and V.M. Velasco, *Solar Physics*, **271**, 169–182 (2011).  
 [8] V.M. Velasco, B. Mendoza, and J.F. Valdés-Galicia, *Proceedings of the 30th International Cosmic Ray Conference*, **1** (SH), 553–556 (2008).  
 [9] S.M. Tobias, N.O. Weiss, and J. Beer., *Astron. Geophys.*, **45**, 2.6 (2004).  
 [10] G. E. Hale, *The Astrophysical Journal.*, **28**, 315–343 (1908).  
 [11] M.S. Kirk, M.S. and W.D. Pesnell and C.A. Young and S.A. Hess-Webber, *Solar Physics*, **257**, 99–112 (2009).  
 [12] C.O. Lee, *Solar Physics*, **256**, 345–363 (2009).  
 [13] E.J. Smith and A. Balogh, *Geophys. Res. Lett.*, **35**, L22103 (2008).  
 [14] D.J. McComas et al., *Geophys. Res. Lett.*, **35**, L18103 (2008).  
 [15] C. Fröhlich, *Astron. Astrophys.*, **501**, L27–L30 (2009).  
 [16] C. Fröhlich, *Space Sci. Rev.*, **125**, 53–65 (2006).  
 [17] P. C. Foukal, H. Fröhlich, Spruit, and T.M.M. Wigley, *Geophys. Res. Lett.*, **36**, L19704 (2009).  
 [18] I.G. Usoskin, S.K. Solanki, M. Schussler, K. Mursula, and K. Alanko, *Phys. Rev. Lett.*, **91**, 211101, 211101 (2003).  
 [19] M. Lockwood and A.P. Rouillard and I.D. Finch, *Astrophys. J.*, **700**, 937–944 (2009).  
 [20] J.A. Abreu et al., *Geophys. Res. Lett.*, **48**, RG2004 (2010).  
 [21] C.T. Russell, J.G. Luhmann, and L.K. Jian., *Rev. Geophys.*, **320**, 735–738 (1986).  
 [22] N.R. Rigozo et al., *Planetary and Space Sci.*, **58**, 1971–1976 (2010).  
 [23] W.D. Pesnell, *Living Rev. Solar Phys.*, **7**(6) (2008).  
 [24] V. Vapnik, *Statistical Learning Theory* (Jhon Wiley & Sons, New York., 1998).  
 [25] J.A.K. Suykens, T.V. Gestel, J. De Brabanter, B. De Moor, and J. Vandewalle, *Least-Squares Support Vector Machines* (World Scientific Publishing Co. Pte. Ltd, 2005).  
 [26] A.I. Steinhilber, J. Beer, and C. Fröhlich, *Geophys. Res. Lett.*, **36**, L19704 (2009).  
 [27] A.I. Shapiro et al, *Astron. Astrophys.*, **529**, A67 (2011).  
 [28] L.J. Gray, et al, *Rev. Geophys.*, **48**, RG4001 (2010).  
 [29] Y-M. Wang, J. L. Lean, and N.R. Sheeley Jr., *Astrophys. J.*, **625**, 522–538 (2005).  
 [30] K.E. Taylor, R.J. Stouffer, and G.A. Meehl, <http://cmip-pcmdi.llnl.gov/cmip5/docs/TaylorCMIP5design.pdf> (2009).  
 [31] N.A. Krivova, L.E.A. Vieira, and S.K. Solanki., *Journal of Geophysical Research*, **115**, A12112, 11 (2010).  
 [32] C. Torrence and G.P. Compo, *Bull. Am. Meteorol. Soc.*, **79**, 61–78 (1998).  
 [33] W. Soon et al., *Journal of Atmospheric and Solar-Terrestrial Physics*, **73**, 2331–2344 (2011).  
 [34] A. Grinsted, J. Moore, and S. Jevrejera, *Nonlinear Process. Geophys.*, **11**, 561566 (2004).  
 [35] C. Torrence and P. Webster, *J. Clim.*, **12**, 2679–2690. (1999).  
 [36] V.M. Velasco and B. Mendoza, *Advances in Space Research*, **12**, 866–878 (2008).  
 [37] D.L. Gilman, F.H. Fuglister, and J.M. Mitchell, *J. Atmos. Sci.*, **20**, 182–184 (1963).  
 [38] J. Beer, S.M. Tobias, and N.O. Weiss, *Solar Physics*, **181**, 237–249 (1998).